



Preliminary neutron study of a thorium-based molten salt energy amplifier

Pu Yang^{1,2} · Zuo-Kang Lin¹ · Wei-shi Wan³ · Gui-Feng Zhu¹ ·
Xiao-Han Yu¹ · Zhi-Min Dai¹

Received: 18 November 2019 / Revised: 11 February 2020 / Accepted: 12 February 2020 / Published online: 19 March 2020
© China Science Publishing & Media Ltd. (Science Press), Shanghai Institute of Applied Physics, the Chinese Academy of Sciences, Chinese Nuclear Society and Springer Nature Singapore Pte Ltd. 2020

Abstract Present designs for molten salt thermal reactors require complex online processing systems, which are technologically challenging, while an accelerator-driven subcritical molten salt system can operate without an online processing system, simplifying the design. Previous designs of accelerator-driven subcritical systems usually required very high-power proton accelerators (> 10 MW). In this research, a proton accelerator is used to drive a thorium-based molten salt fast energy amplifier (TMSFEA) that improves the neutron efficiency of the system. The research results show that TMSFEA can achieve a long-term stable state for more than 30 years with a rated power of 300 MW and a stabilizing effective multiplication factor (k_{eff}) without any online processing. In this study, a physical design of an integrated molten salt energy amplifier with an initial energy gain of 117 was accomplished. According to the burn-up calculation, a molten salt energy amplifier with the rated power of 300 MW_{th} should be able to operate continuously for nearly 40 years using a

1 GeV proton beam below 4 mA during the lifetime. By the end of the life cycle, the energy gain can still reach 76, and ^{233}U contributes 70.9% of the total fission rate, which indicates the efficient utilization of the thorium fuel.

Keywords Molten salt · Energy amplifier · Energy gain · Conversion ratio · Beam intensity

1 Introduction

The concept of an energy amplifier (EA) was proposed by Rubbia et al. [1]. It is designed for continuous clean energy production from abundantly available materials using the simplest means and producing a minimal amount of radioactive waste. Considering the linearly growing accumulation of plutonium, which can cause nuclear proliferation problems, the EA further explores the possibilities of plutonium incineration by using a thorium–plutonium mixture [2]. Based on the concept of EA, many similar systems have been developed, aiming at nuclear waste transmutation or fuel breeding, referred to as accelerator-driven system (ADS) [3–5]. Although Rubbia's EA and many other ADSs use solid fuel, a few ADSs based on molten salt fuel have also been proposed [6–10] because solid fuel has prohibitive power peaking problems.

Molten salt fuel is based on the dissolution of fissile materials in an inorganic liquid. It is a family of liquid fuels that serves as both fuel and coolant in molten salt reactors (MSRs). Molten salt as a liquid fuel has some potential advantages compared to conventional solid fuel rods, such as avoiding the complex solid fuel fabrication/refabrication process, adjustable fuel composition, fuel reprocessing without shutting down the reactor, operating at a higher

This work was supported by the Chinese TMSR Strategic Pioneer Science and Technology Project (No. XDA02010000), and the Frontier Science Key Program of the Chinese Academy of Sciences (No. QYZDY-SSW-JSC016).

✉ Zuo-Kang Lin
linzuokang@sinap.ac.cn

✉ Wei-shi Wan
wanwsh@shanghaiTech.edu.cn

¹ Shanghai Institute of Applied Physics, Chinese Academy of Sciences, Shanghai 201800, China

² University of Chinese Academy of Sciences, Beijing 100049, China

³ ShanghaiTech University, Shanghai 201210, China

temperature, and thus raising the efficiency of thermo-electric conversion. Since the concept of molten salt fuel was proposed, MSR studies were mostly based on either molten fluoride-based or chloride-based salt. Both types of these fuel salts have good heat capacity and are chemically stable. But there are some obvious differences between fluoride and chloride molten salts. Compared with chlorine, fluorine has a smaller neutron absorption cross section; thus, it is a more effective moderator of neutrons. Therefore, fluoride-based molten salts are commonly used in thermal reactor design, while chloride-based molten salts are mostly applied as fuel salts for fast reactors. In recent years, many MSR concepts have been proposed, such as the molten salt fast reactor (MSFR) [11], molten salt actinide recycler and transmuter (MOSART) [12], stable salt reactor (SSR) [13], dual fluid reactor (DFR), [14], and a small modular molten salt reactor (SMMSR) [15, 16]. In 2011, a thorium-based molten salt reactor program (TMSR) [17] was initiated in China, which aims to develop both solid and liquid fueled MSRs within 20–30 years in order to achieve efficient use of thorium energy [18–20].

Concepts that combine ADS and molten salt fuel arose in the 1980s. In these concepts, molten salts are mostly presented as solutions for transmutation and thorium utilization purposes. Furukawa et al. [21–23] developed an accelerator molten salt breeder (AMSB) for the production of fissile fuel by application of molten fluorides. Since the early 1990s, Bowman et al. [24] have designed different molten salt systems for accelerator-driven transmutation of nuclear wastes: Two-stage molten salt systems, the so-called Tier 1 and Tier 2, were proposed. Tier 1 is a once-through accelerator-driven transmutation based on NaF–ZrF₄ molten salt. The actinide remnants from Tier 1 operation will be fed into Tier 2, which acts as a final accelerator-driven transmuter. Unlike the Tier 1 system, Tier 2 is based on Li–Be fluoride salts. The French Alternative Energies and Atomic Energy Commission (CEA) proposed a concept of a thorium-based accelerator-driven subcritical system, called TASSE (Thorium based Accelerator-driven System with Simplified fuel cycle for long term Energy production), to transmute transuranium (TRU) and produce power [25]. TASSE is also based on fluoride molten salts. For the use of chloride-based molten salts, the Japan Atomic Energy Research Institute (JAERI) has developed a conceptual design of an accelerator-driven nuclear waste transmuter based on a chloride-based molten salt target/blanket system [26]. The molten salt acts as both fuel coolant and spallation target. A mixture of NaCl–PuCl₃–MACl₃ (where MA represents Np, Am, and Cm) was chosen for the molten salt system, because chloride molten salts have a higher actinide solubility than fluoride molten salts.

In this paper, which combines the concepts of Rubbia's EA and accelerator-driven subcritical molten salt systems, a conceptual design of thorium-based molten salt fast EA (TMSFEA) is proposed. The main concerns of TMSFEA design are stable high energy gain and efficient thorium utilization. A ternary molten salt NaCl–PuCl₃–ThCl₄ is chosen for the molten salt system of TMSFEA, because plutonium has a much higher η (the number of neutrons produced by fissions in fissile nuclides) than uranium in the fast neutron region ($E > 100$ keV). The ternary molten salt acts as both fuel coolant and spallation target. To avoid complex fuel reprocessing, a once-through fuel cycle mode is adopted. Previous designs of ADS relied on GeV proton accelerators achieving intensities of several tens of milliamperes, which is by no means a trivial matter under the current technical status of proton accelerators. Therefore, the development timelines of ADS are still unpredictable. In this work, the maximum beam intensity can be limited to 4 mA with a lifetime of almost 40 years, based on our investigation of the proton energy, reflector design, geometrical parameters of the core, composition of the NaCl–PuCl₃–ThCl₄ fuel salt, and burn-up evolution.

The basic physics of EA is introduced in Sect. 2, while the physical modeling is presented in Sect. 3. The calculation methods are given in Sect. 4. The results and discussion are provided in Sect. 5, and the conclusions are drawn in Sect. 6.

2 Basic physics of EA

2.1 Energy gain

The energy gain (G) of an EA is defined as the ratio of the total energy produced in the system to the power of the accelerator beam [27]. The total energy produced by EA can be expressed as

$$P_{\text{tot}} = Z\varphi^* \frac{k_{\text{eff}} i_p \bar{E}_f}{(1 - k_{\text{eff}})\bar{\nu}}, \quad (1)$$

where Z stands for the number of source neutrons generated per incident proton, i_p is the required beam intensity, \bar{E}_f is the average recoverable energy released in a fission, $\bar{\nu}$ is the average number of neutrons produced per fission, and φ^* is the neutron source efficiency, which represents the average importance of external source neutrons over the average importance of fission neutrons [28]. It is defined as

$$\varphi^* = \frac{1 - k_{\text{eff}}}{k_{\text{eff}}} \frac{\bar{\nu} R_f}{S}, \quad (2)$$

where R_f is the fission reaction rate and S is the total production of neutrons by the external source.

By rearranging Eq. 1, the required beam intensity can be expressed as

$$i_p = \frac{P_{acc}}{E_p} = \frac{P_{tot} (1 - k_{eff}) \bar{v}}{Z\varphi^* k_{eff} \bar{E}_f}, \tag{3}$$

where E_p is the proton energy. The power of accelerator beam is $P_{acc} = i_p E_p$. Therefore, the expression of the energy gain is

$$G = \frac{P_{tot}}{P_{acc}} = \frac{Z\varphi^* k_{eff} \bar{E}_f}{E_p (1 - k_{eff}) \bar{v}} \tag{4}$$

Equation 4 shows that the closer k_{eff} is to 1, the larger the energy gain. In addition, it is also advisable to enhance the energy gain by increasing Z and φ^* . For the molten salt spallation target used in the TMSFEA, increasing the content of HM in the molten salt can effectively improve Z and φ^* , thus enhancing the energy gain and decreasing the required proton beam intensity.

2.2 Conversion ratio

The Th–U breeding performance is quantitatively described by the conversion ratio (CR). The CR can be expressed as

$$CR = \frac{R_c^{fertile}}{R_a^{fissile}}, \tag{5}$$

where $R_c^{fertile}$ represents the neutron capture reaction rate of fertile nuclide and $R_a^{fissile}$ stands for the neutron absorption reaction rate of fissile nuclides. For the starting fuel of TMSFEA, the only fissile and fertile nuclides are ^{232}Th , ^{239}Pu , and ^{241}Pu . Therefore, Eq. 5 can be simplified as

$$CR = \frac{R_c(^{232}\text{Th} + ^{240}\text{Pu})}{R_a(^{239}\text{Pu} + ^{241}\text{Pu})}, \tag{6}$$

CR can also be analyzed from the neutron balance point of view. Equation 7 gives the neutron balance in a critical fast reactor [29].

$$CR = \eta + \varepsilon - 1 - (l_A + l_L), \tag{7}$$

where η refers to the number of neutrons produced by fissions in fissile nuclides (per absorbed neutron), ε is the average number of excess neutrons produced by fissions in fertile nuclides, l_A is the number of neutrons absorbed in non-fuel materials, and l_L is the number of neutrons lost by leakage. For the subcritical facility, the contribution of external source neutrons has to be considered, and Eq. 7 becomes

$$CR = \eta + \varepsilon + \mu - 1 - (l_A + l_L), \tag{8}$$

where μ is an external source of neutrons normalized to neutron absorption in fissile nuclides. By applying Eq. 2, μ can be expressed as

$$\mu = \frac{S}{R_a^{fissile}} = \frac{\bar{v}(1 - k_{eff})}{k_{eff}(1 + \alpha)\varphi^*}, \tag{9}$$

where $R_a^{fissile}$ refers to the neutron absorption reaction rate in fissile nuclides and α is the capture–fission ratio. By inserting Eq. 9 into Eq. 8, the expression of CR becomes

$$CR = \eta + \varepsilon + \frac{\bar{v}(1 - k_{eff})}{k_{eff}(1 + \alpha)\varphi^*} - 1 - (l_A + l_L). \tag{10}$$

Equation 10 shows that k_{eff} and CR are two competitive parameters. It is feasible to improve CR by increasing the subcriticality. However, the cost is the necessity to increase the proton beam intensity and decrease the energy gain. It is also noted that η plays an essential role in realizing the breeding ($CR > 1$). From the breeding point of view, η must be large enough (significantly greater than 2). Figure 1 shows the η ratio of four fissile nuclei, namely ^{233}U , ^{235}U , ^{239}Pu , and ^{241}Pu , in the thermal, resonance, and fast regions. It can be seen that η of both nuclei rapidly increases with increasing energy in the fast range ($E > 100$ keV), and ^{239}Pu and ^{241}Pu have the largest η in this region. Therefore, ^{239}Pu and ^{241}Pu have better breeding performance if the average energy of neutron spectrum is higher than ~ 100 keV. As a result, the conversion ratio increases with increasingly harder neutron spectrum. To harden the neutron spectrum, the density of light nuclei in the core should be restricted.

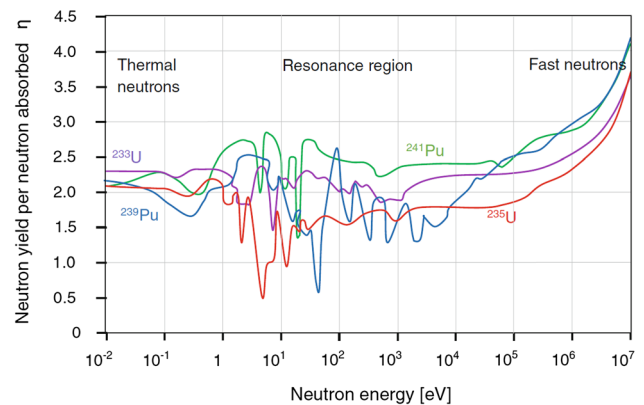


Fig. 1 (Color online) η ratio as a function of the neutron energy for different fissile nuclei

3 Physical modeling

3.1 TMSFEA system

The TMSFEA is an accelerator-driven subcritical single-fluid molten salt system. Instead of achieving a self-sustained chain fission reaction in a critical reactor, TMSFEA uses a subcritical facility to generate energy by introducing extra neutrons produced in the spallation reaction. The general layout of TMSFEA is displayed in Fig. 2. A proton-driver accelerator is coupled to a subcritical facility, and a beam of energetic protons from the accelerator is directly injected into the molten salt, which is held in the reflector, and spallation neutrons are produced to sustain the fission reaction in the subcritical facility. The entire system could be shut down simply by switching off the proton beam rather than inserting any control rods, which makes TMSFEA a much safer system than conventional fission reactors. The fission heat produced in the subcritical core is transferred to the secondary heat exchanger through the primary heat exchanger and then transmitted to the turbine/generator for electricity generation, which can partially be used to run the accelerator.

3.2 Molten salt fuels

One of our primary design goals for TMSFEA is the use of thorium fuel. In a fast neutron subcritical facility, the net ^{233}U production rate from Th with Pu as the starting fuel is much higher than that with U as the starting fuel, because ^{239}Pu and ^{241}Pu have much larger η under the fast spectrum, as described in the previous section. The molten fluoride salt system has been extensively studied for many

years at Oak Ridge National Laboratory as the fuel salt of a molten salt reactor [30] and the target salt of an accelerator-driven transmutation system [7]. However, the solubility of PuF_3 in the fluoride salt is limited, which will seriously affect the loading capacity of Pu in fluoride salts. Moreover, fluorine has a smaller mass number, which is a disadvantage for the neutron spectrum hardening, and thus reduces η of ^{239}Pu and ^{241}Pu . In addition, as a spallation target salt, the fluoride salts have a lower spallation neutron production performance, because the solubility of HM in the fluoride salt is not high enough.

Therefore, a ternary chloride-based molten salt system containing thorium and plutonium was chosen in our design. Molten salts containing thorium and plutonium halides have been widely studied in the nuclear industry since the 1970s, and much research has been conducted regarding their physicochemical characteristics. The results, especially melting diagrams, are the basis of our design. Among these melting diagram results, the $\text{NaCl-PuCl}_3\text{-ThCl}_4$ and the $\text{ThCl}_4\text{-KCl-PuCl}_3$ molten salt systems have a more reasonable melting point for our design. In addition, sodium has a smaller neutron absorption cross section than potassium; therefore, $\text{NaCl-PuCl}_3\text{-ThCl}_4$ was selected as the fuel in our TMSFEA design. Figure 3 illustrates the ternary phase diagram [31] for $\text{NaCl-PuCl}_3\text{-ThCl}_4$ (in mol%), and the expected melting temperature for any mixture of $\text{NaCl-PuCl}_3\text{-ThCl}_4$ is shown. The eutectic point E1 (46.5 mol% NaCl, 18.5 mol% PuCl_3 , and 35.0 mol% ThCl_4) has the lowest melting temperature of 325 °C. Therefore, the range of specific $\text{NaCl-PuCl}_3\text{-ThCl}_4$ fuel salt implementations for any given melting point between 325 and 700 °C is allowed to be investigated. Of particular interest are mixtures having a melting

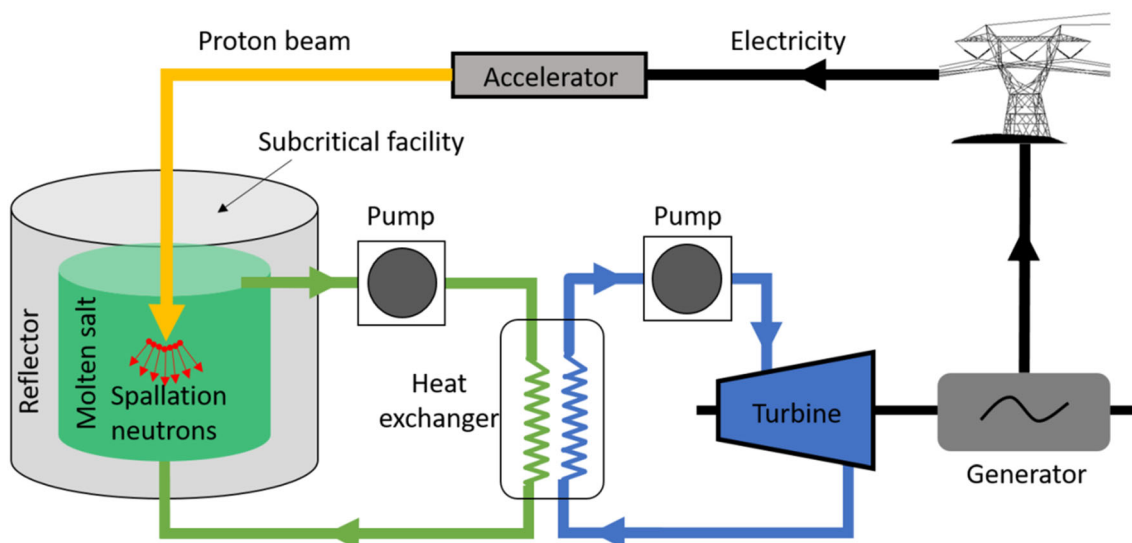


Fig. 2 (Color online) Schematic diagram of TMSFEA

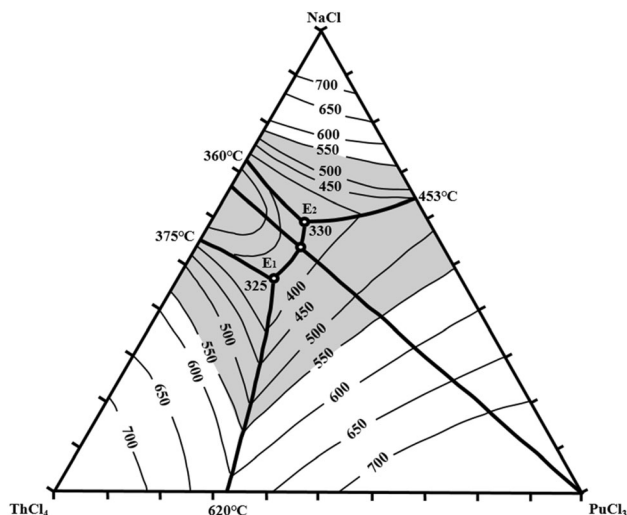


Fig. 3 Phase diagram of NaCl–PuCl₃–ThCl₄

point of less than 550 °C, which are illustrated in the gray region of the ternary phase diagram. Various specific compositions of NaCl–PuCl₃–ThCl₄ fuel salt in the gray region can be used in the TMSFEA. The choice of the final composition depends on a variety of factors, including the spallation neutrons production performance, the energy gain, and the Th–U breeding performance.

As for the material compatibility problem, the majority of chloride-based salts are not aggressively corrosive to stainless steels or nickel-based alloys at a reactor temperature without the presence of oxygen [32]. However, long-term operation requires a high degree of material compatibility, and considerable future research of chloride salts is needed, since most of the available information relates to fluoride-based salts with uranium dissolved inside. In addition, as described in the ORNL report: [33] “in-core testing of material compatibility of structural materials exposed to fuel-bearing chloride salts has yet to be performed, so materials compatibility cannot yet inform the salt selection.”

3.3 Subcritical facility modeling

The schematic of the subcritical facility of TMSFEA is shown in Fig. 4. To simplify the core structure, a single-fluid type design is adopted. The average operating temperature of fuel salt is 963 K, which refers to the design of REBUS-3700 [34]. The fuel salt is poured into a cylindrical core barrel which is made of Hastelloy-N with a 2 cm thickness. A reflector was employed to reduce the leakage of neutrons. A 5-cm-thick Hastelloy-N vessel is placed outside the reflector. A proton beam is transported in a 1-cm-thick Hastelloy-N tube and is injected into the core. The outer diameter of the beam tube is 20 cm, which refers

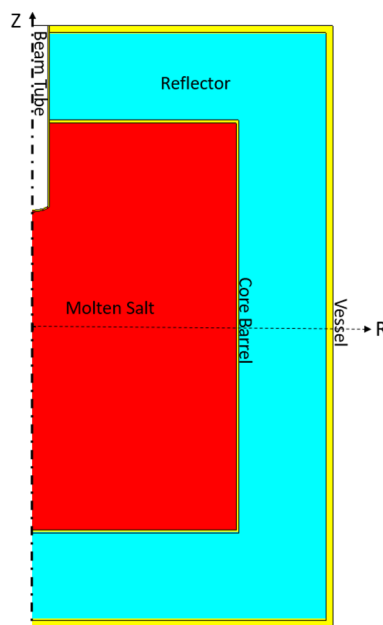


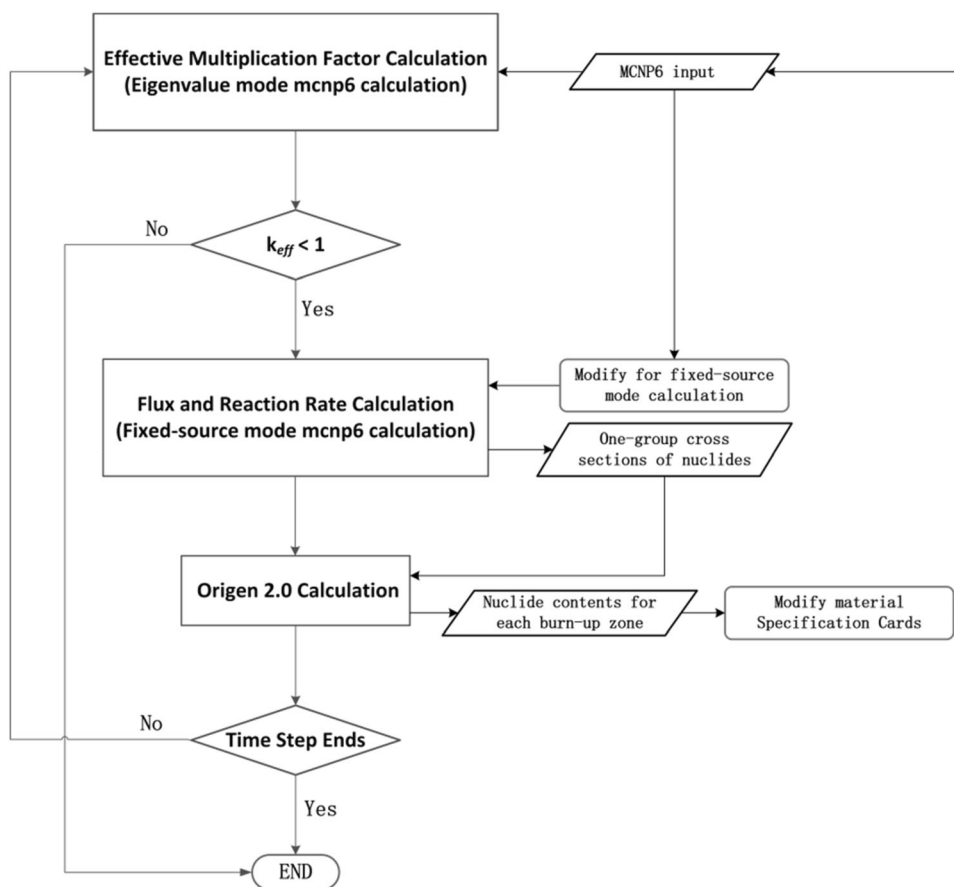
Fig. 4 (Color online) Schematic diagram of the subcritical facility model

to the beam tube design of Rubbia’s EA [1]. In addition, initially, the plutonium in the ternary molten salt system consists of about 1.9 wt% ²³⁸Pu, 58.6 wt% ²³⁹Pu, 23.8 wt% ²⁴⁰Pu, 10.2 wt% ²⁴¹Pu, and 5.5 wt% ²⁴²Pu, which is considered to be a typical isotopic composition of plutonium recovered from PWR spent fuel [35].

4 Calculation methods

In this work, the Monte Carlo code MCNP6.1 [36] was used for our main calculations, and the point burn-up code ORIGEN2.0 [37] was employed for depletion and decay calculations. The intra-nuclear cascade physics model INCL coupled with the ALBA evaporation model in MCNP6.1 was used for high-energy nuclear reactions. The evaluated nuclear data library ENDF/B-VII.1 was used for neutron energies up to 150 MeV. MCNP6.1 has two calculation modes, one of which is an eigenvalue mode by using Kcode card, and the other is a fixed-source mode. In our calculations, only the subcriticality factor *k_{eff}* was calculated using the KCODE mode, while in all other calculations the fixed-source mode in MCNP6.1 was adopted.

The flowchart of the burn-up calculation process is presented in Fig. 5. The burn-up calculation was implemented using MCNP6.1 and ORIGEN2.0. First, examining whether *k_{eff}* is less than 1 using KCODE calculations, and if not, ending the calculation or calculating the fluxes and one-group cross sections of burn-up regions using a fixed-

Fig. 5 Flowchart of the calculation

source mode, then ORIGEN2.0 calculations are carried out to get new compositions for each burn-up region for the next time step. After that, the density and composition of the molten salt in MCNP6.1 input card need to be modified, and a new round of iterative calculation begins until the iteration condition is not satisfied (k_{eff} greater than 1 or the total number of total burn-up steps is exceeded).

To test our calculation method, the ADS benchmark problem of the International Atomic Energy Agency (IAEA), which is a thorium-based subcritical reactor model, [38] was analyzed. The evolution of the effective multiplication factor and the intensity of an external source (can be converted into beam intensity) evolution is investigated. The comparison results are shown in Fig. 6. The black lines are our results, the red lines are the outcomes of the Japan Atomic Energy Research Institute (JAERI), and the blue ones are from the Karlsruhe Institute of Technology (KIT). For k_{eff} evolution, the black line shows a good agreement with other results. Due to differences in the calculation programs and the nuclear data library, there are still some differences in those curves, but they have the same variation trend. In addition, our results are closer to those from the JAERI, since both of them are based on the Monte Carlo method. Regarding the evolution of the

intensity of the external source, since KIT did not provide any relevant calculation results, we only compared the calculation results with the JAERI data, and they also show good agreement. Therefore, the calculation method can be used in the TMSFEA investigation.

5 Results and discussion

5.1 Optimization of TMSFEA design parameters

According to Eq. 4, the amount of energy gain depends on the proton energy E_p , performance of the spallation target (i.e., Z and φ^*), and the characteristics of the subcritical facility (i.e., k_{eff} , \bar{E}_f , and $\bar{\nu}$). The value of \bar{E}_f is mainly determined by the fission nuclides of the fuel and can be considered constant when the proton energy varies [39]. For the starting fuel of TMSFEA, the only fissile nuclides are ^{239}Pu and ^{241}Pu . The values of \bar{E}_f for ^{239}Pu and ^{241}Pu are 199.88 MeV and 201.88 MeV, respectively [40]. In this work, the compromise value of 200 MeV was chosen for the energy gain calculation.

For a fixed core structure and molten salt composition, the variation of energy gain with proton energy was

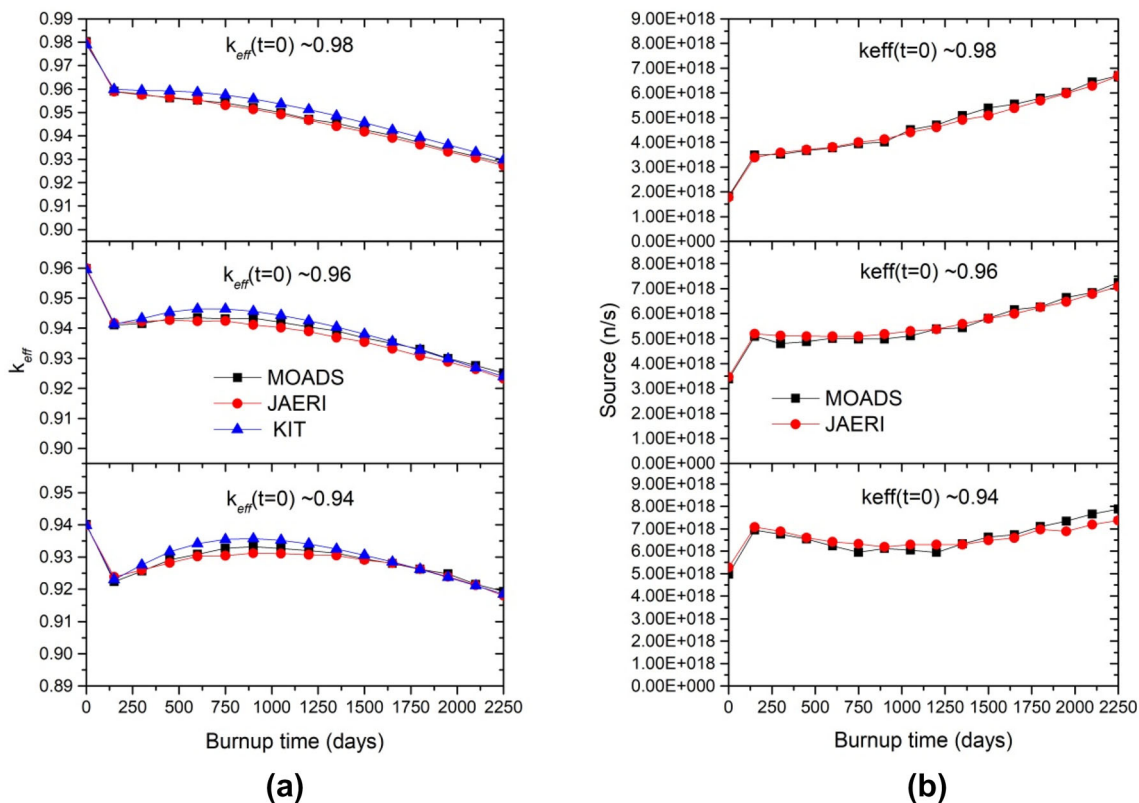


Fig. 6 (Color online) Results of IAEA-ADS benchmark. **a** Evolution of k_{eff} , **b** evolution of source intensity

calculated. In Fig. 7, the energy gain is plotted as a function of the energy of the incident proton. The results show that the energy gain increases rapidly with increasing proton energy up to about 1000 MeV and reaches the maximum value at about 1600 MeV. Table 1 gives the specific values of Z , φ^* , $\bar{\nu}$, and energy gain G . As shown in Table 1, the value of $\bar{\nu}$ is hardly changed with the proton energy, since $\bar{\nu}$ is determined by the fuel composition. When the proton energy is below 1000 MeV, φ^* increases

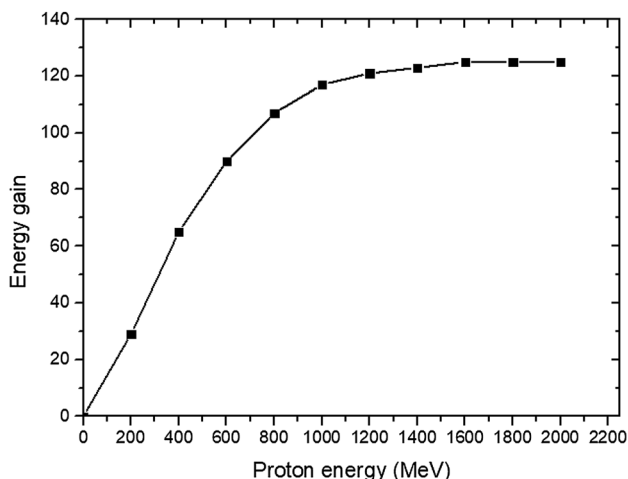


Fig. 7 Energy gain as a function of proton energy for proton beams

Table 1 Dependence of neutron parameters on proton beam energy

Proton energy (MeV)	Z	φ^*	$\bar{\nu}$	G
400	4.89	1.62	2.99	65
600	9.80	1.69	2.99	90
800	15.18	1.71	2.99	106
1000	20.49	1.72	2.99	116
1600	35.49	1.72	2.99	125
1800	39.89	1.72	2.99	125
2000	44.24	1.72	2.99	125

with the proton energy enhancement, which is due to the larger production of high-energy neutrons, which can produce more fission neutrons. However, when the proton energy is greater than 1000 MeV, φ^* does not vary with the proton energy, which is mainly due to the increasing cross section of pion generation and the difficulty of producing higher energy neutrons. It is also noted that when the proton energy is increased from 1000 to 1600 MeV (an increase of 60%), the energy gain increases only by 8%. Therefore, from the economic perspective, the proton energy of 1000 MeV is chosen in our design.

The subcriticality factor k_{eff} also has a significant impact on the energy gain. The closer the neutron multiplication factor to 1, the greater the energy gain. However, the choice of k_{eff} is mainly based on the consideration of safety. A reasonable subcriticality margin should be considered to avoid a critical accident at a subcritical facility. Therefore, the initial k_{eff} value was set to 0.98 in our design.

In addition to the energy gain, another concern of TMSFEA is the Th–U breeding performance. As shown in Eq. 10, the Th–U breeding performance can be enhanced by reducing the leakage ratio. There are two ways to reduce the leakage ratio: one is to arrange a reflector, and the other is to increase the core size. To assess the influence of the reflector on CR, the initial CRs of different layouts of reflector are calculated and shown in Fig. 8. Unlike the monotonic increase in CR for a lead reflector, with an increase in the graphite reflector thickness, CR tends to increase first and then to decline when the thickness is larger than 10 cm. As shown in Fig. 9, the tendency to increase CR for the graphite reflector is due to the larger positive contribution of l_L . After 10 cm, a significant increase in l_A leads to a decrease in CR, since the softened spectrum increases the neutron absorption by non-fuel nuclides. Furthermore, CR for both reflectors becomes almost steady when the thickness is larger than 60 cm.

Figure 10 shows the neutron spectra of the core for different reflector arrangements; the layout of reflectors can significantly soften the neutron spectrum, especially for graphite. It can be noticed that even 10 cm of graphite has a softer spectrum compared to lead with the thickness of 90 cm, which explains the variation trend of the neutron parameters, as shown in Fig. 8. Considering that the breeding of thorium in a plutonium-started core needs a

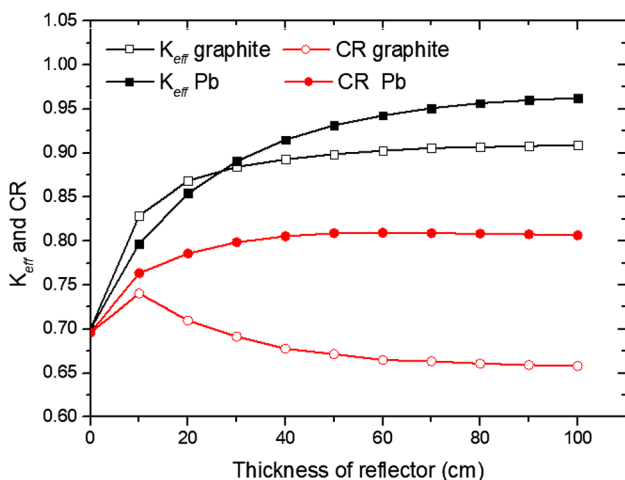


Fig. 8 (Color online) Initial CR and k_{eff} for different reflector arrangements

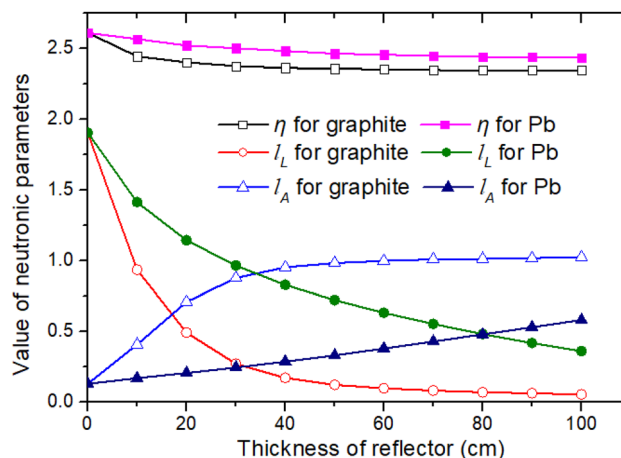


Fig. 9 (Color online) Neutron parameters as the functions of the thickness of different reflectors

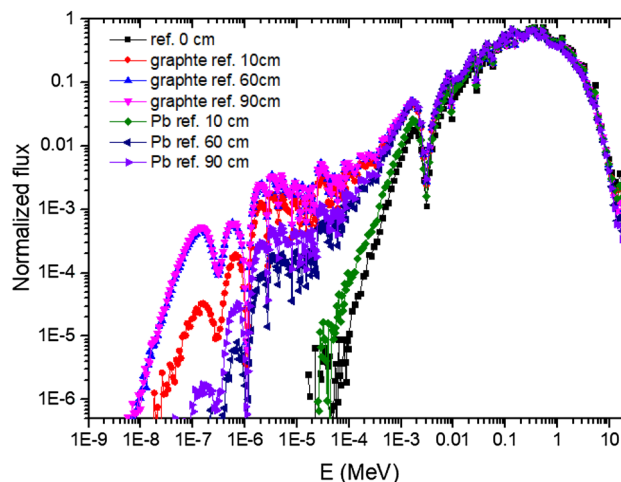


Fig. 10 (Color online) Neutron spectrum for different reflector arrangements

harder neutron spectrum, a lead reflector is more suitable for our design.

An increase in the core size can also reduce leakage ratio. The height–diameter ratio of the core is fixed to 1. Figure 11 shows that CR and k_{eff} change as the core size is increased. The larger the core, the lower the neutron leakage and, consequently, the higher the k_{eff} and CR. Furthermore, enlarging the core barely has any effect on the spectrum or spectrum-related parameters (i.e., η , l_A , μ , and ε).

The composition of NaCl–PuCl₃–ThCl₄ fuel is also optimized to meet the criticality and the CR requirements for long-term operation of the EA system. Based on the above analysis, a 60-cm liquid lead reflector was chosen. In order to keep a subcritical state and achieve breeding, k_{eff} is set to 0.98, and CR should be above 1. These conditions can be used to determine a relatively reasonable fuel salt composition. Figure 12 shows the variation of CR for different fuel

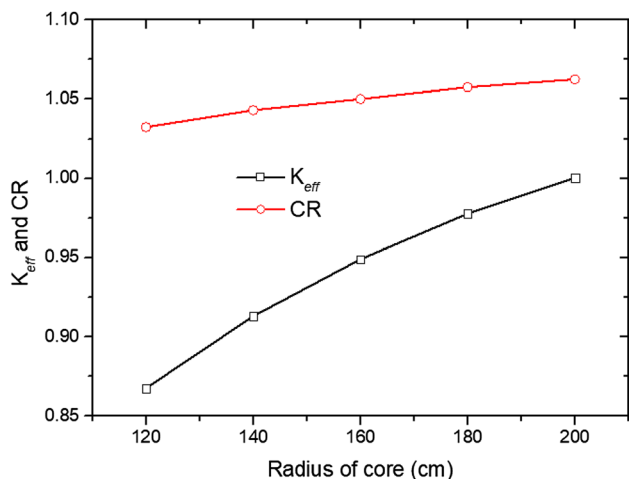


Fig. 11 (Color online) Initial CR and k_{eff} for different core sizes

salt compositions. There is no adaptive area in Fig. 12a, which means that the 120 cm radius core does not satisfy the breeding condition. When the radius of the core is set to 150 cm in Fig. 12b, the contour line of $k_{eff} = 0.98$ intersects with the region $CR > 1$ satisfying the breeding condition of the EA. The composition marked with a star in Fig. 12b is chosen in the molten salt EA design because it has a reasonable CR and melt temperature (~ 530 °C).

After the optimization, the main parameters of TMSFEA are listed in Table 2.

5.2 Burn-up analysis

The evolution of TMSFEA k_{eff} and beam intensity with three different kinds of thermal power is displayed in

Fig. 13. A 300 MW_{th} facility has the steadiest k_{eff} , and thus a relatively gentle evolution of the beam intensity compared to the other two kinds of cases with higher power. At a rated power, TMSFEA is expected to have a steady energy gain; namely, it meets the stable beam intensity requirement during the operation. As can be seen from Eq. 3, the beam intensity of TMSFEA is mainly affected by k_{eff} , Z , \bar{E}_f , \bar{v} , and ϕ^* . Except for k_{eff} , variations in other terms are small.

The k_{eff} evolution is associated with CR, which must be higher than approximately 1.03 to maintain stability in cases of Pu–Th loading, since η for Pu is about 1.03 times higher than that of ^{233}U in this spectrum. Taking the thermal power of 1 GW as an example, the value of k_{eff} monotonically decreases when CR is below 1.03 after 5 years. In addition, due to the effect of Pa, k_{eff} shows a rapid decline in a few days after the beginning, which results in an increase in beam intensity at the beginning of the operation. It is also worth noting that the CR of 1 GW thermal power drops to a minimum value (~ 0.89) and then has a certain increase, which is due to the increased contribution of the external neutron source.

The evolution of the Pu and ^{233}U at thermal powers, 300 MW_{th} and 500 MW_{th}, is presented in Fig. 14. As the contribution of ^{233}U to the total fission rate increases, the net production rate of ^{233}U will gradually decrease. The net ^{233}U production at 500 MW_{th} thermal power starts decreasing after 45 years, since ^{233}U contributes about 85% of the total fission rate, which can greatly increase the consumption of ^{233}U .

Under different beam intensity restrictions, the production of ^{233}U and the amount of Pu transmutation are given in Table 3. The results indicate that the lifetime is much longer for 300 MW_{th}. For a maximum beam intensity limit of 6 mA, the lifetime of TMSFEA for 300 MW_{th} and 500

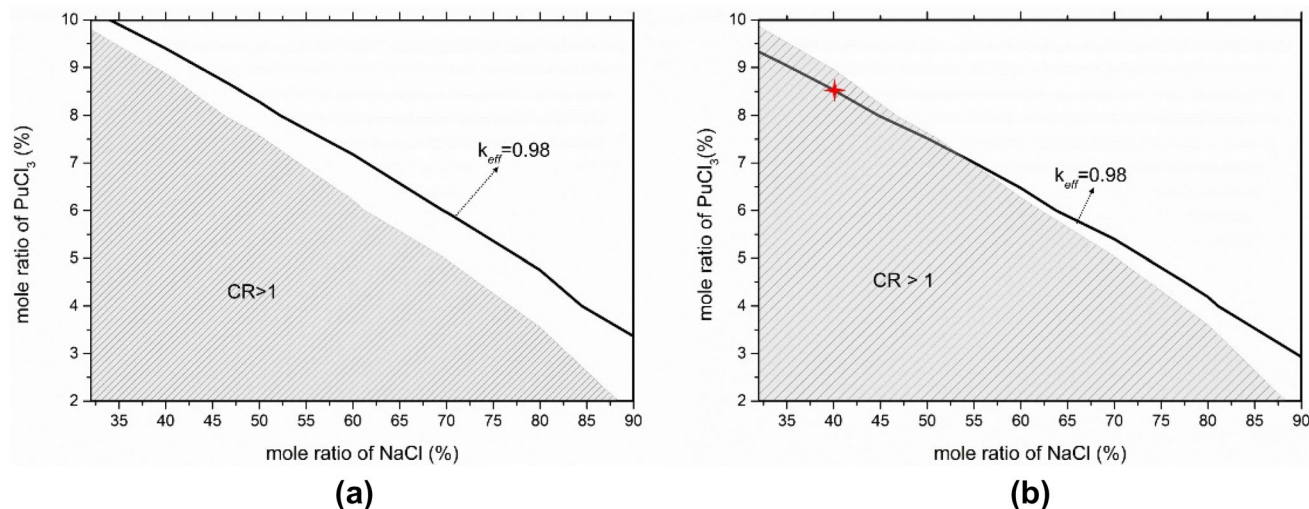
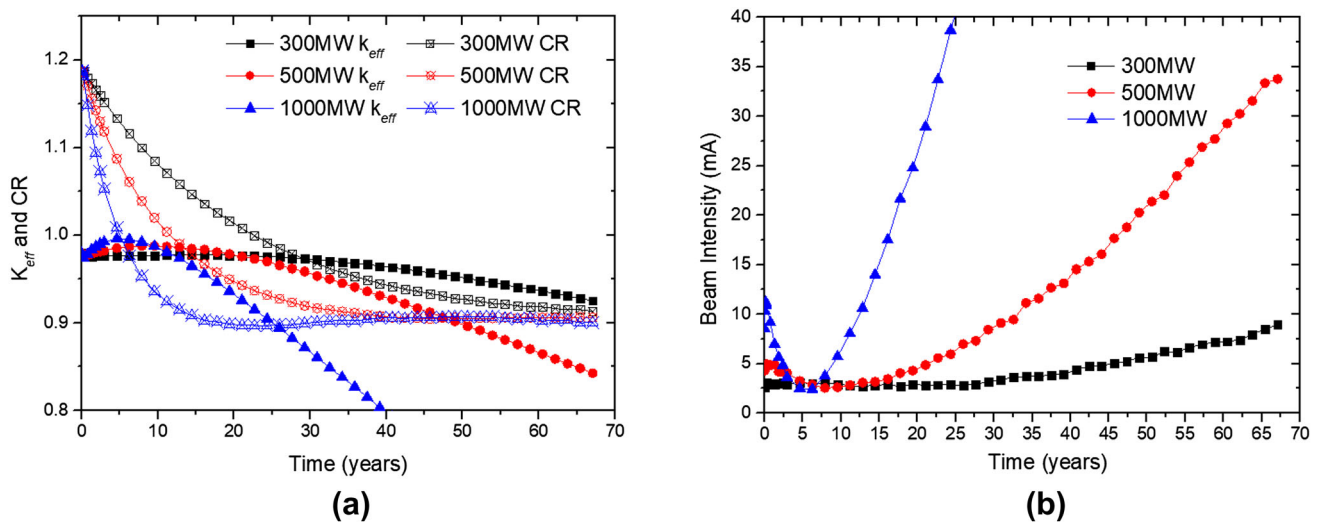


Fig. 12 CR as a function of fuel salt composition. **a** The radius of the core is 120 cm, **b** the radius of the core is 150 cm

Table 2 Main design parameters of TMSFEA

Parameters	Value
Initial subcriticality factor k_{eff}	0.98
Proton energy (GeV)	1
Beam tube external diameter (cm)	20
Window material	Hastelloy-N alloy
Beam radius at spallation target (cm)	7.5
Initial fuel composition (mole ratio %)	40.0NaCl-8.5PuCl ₃ -51.5ThCl ₄
Fuel salt volume (m ³)	21.2
Initial Pu/Th loading (t)	5.7/33.5
Average fuel temperature	963 K
Doppler reactivity coefficient (pcm/k)	- 0.65
Void coefficient (pcm/k)	- 10.56
Reflector material	Liquid lead
Reflector thickness (cm)	60
Energy gain	117

**Fig. 13** (Color online) Time evolution of k_{eff} , CR, and beam intensity. **a** Evolution of k_{eff} and CR, **b** evolution of beam intensity

MW_{th} is 51 and 24 years, respectively. At the end of the service life, about 57% of Pu and 16% of Th were consumed at 300 MW_{th} , compared with 50% and 13% at 500 MW_{th} . Furthermore, the net production of ^{233}U is 7% higher at 300 MW_{th} than at 500 MW_{th} . With the maximum beam intensity limit of 4 mA, the lifetime of TMSFEA at 300 MW_{th} is 39 years, and the maximum fission rate contribution of ^{233}U is 70.9%, which indicates the efficient thorium utilization. At the end of the life cycle at 300 MW_{th} with a 4 mA limit, the energy gain is 76, while that with a 6 mA limit is 53. Therefore, TMSFEA is recommended to operate at 300 MW with a 4 mA beam intensity limit, because the energy gain can be maintained at a higher level.

6 Conclusion

To assess the stable high energy gain and thorium utilization with a lower beam intensity requirement in the accelerator-driven system, a preliminary physical design of TMSFEA is proposed, and the design parameters are optimized by investigating the proton energy, reflector design, geometrical parameters of the core, fuel salt composition, and burn-up evolution. Conclusions drawn from the above analyses are presented below.

When using the NaCl–PuCl₃–ThCl₄ ternary molten salt system as a spallation target, the energy gain rapidly increases with an increase in proton energy up to about 1000 MeV. The energy gain slightly increases when the

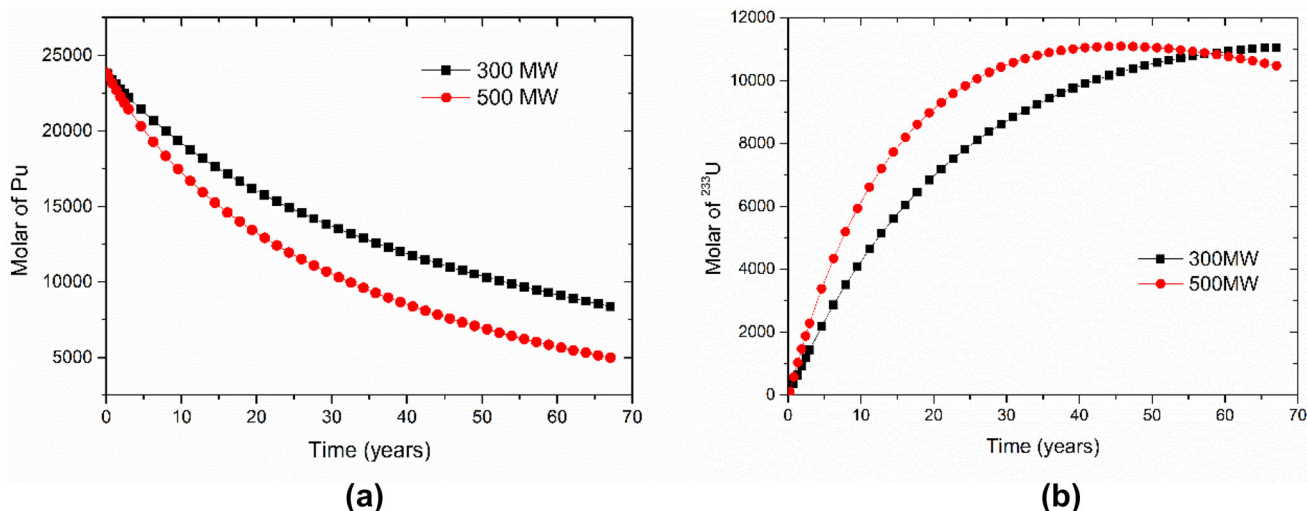


Fig. 14 (Color online) Evolution of Pu and ²³³U. **a** Evolution of Pu, **b** evolution of ²³³U

Table 3 Burnup results for different thermal powers under different beam intensity restrictions

Maximum beam intensity limit (mA)	4		6		8	
Thermal power (MW)	300	500	300	500	300	500
Lifetime (years)	39	N/A*	51	24	64	28
Total Th consumption (kg)	4381.3	N/A	5539.1	4495.0	6838.2	5318.6
Net ²³³ U production (kg)	2273.6	N/A	2460.2	2293.0	2563.0	2389.8
Total Pu consumption (kg)	2828.5	N/A	3239.6	2843.3	3621.0	3036.3

*N/A means the starting beam intensity requirement exceeds 4 mA

proton energy is greater than 1000 MeV. Therefore, 1000 MeV is a more reasonable energy for the incident proton. A reflector can effectively reduce neutron leakage, but it can also soften the neutron spectrum of the core. Compared to a graphite reflector, a liquid lead reflector moderates the neutron spectrum somewhat less, which is more suitable for the design of TMSFEA. By changing the core size and the composition of NaCl–PuCl₃–ThCl₄ fuel, the main parameters of TMSFEA are obtained, which yields an initial energy gain of 117. Based on our design, burn-up analyses are carried out at three thermal power levels. With a maximum beam intensity limit of 4 mA, the lifetime of TMSFEA at 300 MW_{th} is 39 years. By the end of the life cycle, energy gain can still reach 76, and ²³³U contributes 70.9% of the total fission rate, which indicates the efficient thorium utilization.

The present work is mainly focused on a one generation system that is launched using plutonium fuel. However, there are plenty of available actinides in the discharged fuel of the TMSFEA. By removing the fission products from the end of cycle of the previous generation TMSFEA fuel, only fresh thorium must be added to the fuel to start the next

generation TMSFEA. To further enhance the thorium utilization, a multi-generation TMSFEA will be studied in our future work.

References

1. C. Rubbia, C. Roche, J.A. Rubio, et al. Conceptual design of a fast neutron operated high power energy amplifier. Internal Report CERN. Switzerland: CERN, 1995. (Report No.: CERN-AT-95-44-ET)
2. C. Rubbia, S. Buono, E. Gonzalez, et al. In A realistic Plutonium Elimination Scheme with Fast Energy Amplifiers and Thorium-Plutonium Fuel, in *Advanced Nuclear Systems Consuming Excess Plutonium*, ed. by E.R. Merz, C.E. Walter (Springer, Dordrecht, 1997), pp. 89–134
3. H. Nifenecker, S. David, J.M. Loiseaux et al., Basics of accelerator driven subcritical reactors. Nucl. Instrum. Methods Phys. Res., Sect. A. **463**(3), 428–467 (2001). [https://doi.org/10.1016/S0168-9002\(01\)00160-7](https://doi.org/10.1016/S0168-9002(01)00160-7)
4. P.A. Gokhale, S. Deokattey, V. Kumar, Accelerator driven systems (ADS) for energy production and waste transmutation: international trends in R&D. Prog. Nucl. Energy **48**(2), 91–102 (2006). <https://doi.org/10.1016/j.pnucene.2005.09.006>
5. W. Maschek, X. Chen, F. Delage et al., Accelerator driven systems for transmutation: fuel development, design and safety.

- Prog. Nucl. Energy **50**(2–6), 333–340 (2008). <https://doi.org/10.1016/j.pnucene.2007.11.066>
6. P. McIntyre, S. Assadi, K. Badgley et al., Accelerator-driven subcritical fission in molten salt core: Closing the nuclear fuel cycle for green nuclear energy. AIP Conf. Proc. **1525**(1), 636–642 (2013). <https://doi.org/10.1063/1.4802405>
 7. C.D. Bowman, E.D. Arthur, P.W. Lisowski et al., Nuclear energy generation and waste transmutation using an accelerator-driven intense thermal neutron source. Nucl. Instrum. Methods Phys. Res., Sect. A. **320**(1–2), 336–367 (1992). [https://doi.org/10.1016/0168-9002\(92\)90795-6](https://doi.org/10.1016/0168-9002(92)90795-6)
 8. A.M. Degtyarev, A.K. Kalugin, L.I. Ponomarev, Cascade subcritical molten salt reactor (CSMSR): main features and restrictions. Prog. Nucl. Energy **1**(47), 99–105 (2005). <https://doi.org/10.1016/j.pnucene.2005.05.008>
 9. X.C. Zhao, D.Y. Cui, X.Z. Cai et al., Analysis of Th–U breeding capability for an accelerator-driven subcritical molten salt reactor. Nucl. Sci. Tech. **29**, 121 (2018). <https://doi.org/10.1007/s41365-018-0448-3>
 10. X.C. Zhao, X.Z. Cai, J.G. Chen, Study of the neutronics performance of molten salt fuel in an accelerator driven subcritical reactor. Nucl. Tech. **41**(8), 080601 (2018). <https://doi.org/10.11889/j.0253-3219.2018.hjs.41.080601>. (in Chinese)
 11. E. Merle-Lucotte, M. Allibert, M. Brovchenko et al., *Introduction to the physics of thorium molten salt fast reactor (MSFR) concepts. Thorium Energy for the World* (Springer, Cham, 2016), pp. 223–231. https://doi.org/10.1007/978-3-319-26542-1_34
 12. V. Ignatiev, O. Feynberg, I. Gnidoi, et al. Progress in development of Li, Be, Na/F Molten salt actinide recycler & transmuter concept, in *Proceeding of ICAPP*, Nice, France (2007)
 13. IAEA. Advances in small modular reactor technology developments, in *IAEA Advanced Reactors Information System (ARIS)* (2018), pp. 217–220
 14. A. Huke, G. Ruprecht, D. Weißbach et al., The dual fluid reactor—a novel concept for a fast nuclear reactor of high efficiency. Ann. Nucl. Energy **80**, 225–235 (2015). <https://doi.org/10.1016/j.anucene.2015.02.016>
 15. G.F. Zhu, Y. Zou, R. Yan et al., Low enriched uranium and thorium fuel utilization under once-through and offline reprocessing scenarios in small modular molten salt reactor. Int. J. Energy Res. **43**(11), 5775–5787 (2019). <https://doi.org/10.1002/er.4676>
 16. M.L. Tan, G.F. Zhu, Y. Zou et al., Research on the effect of the heavy nuclei amount on the temperature reactivity coefficient in a small modular molten salt reactor. Nucl. Sci. Tech. **30**, 140 (2019). <https://doi.org/10.1007/s41365-019-0666-3>
 17. X.Z. Cai, Z.M. Dai, H.J. Xu, Thorium molten salt reactor nuclear energy system. Physics **45**(9), 578–590 (2016). <https://doi.org/10.7693/wl20160904>. (in Chinese)
 18. S.H. Yu, Y.F. Liu, P. Yang et al., Effect analysis of core structure changes on reactivity in molten salt experimental reactor. Nucl. Tech. **42**(02), 020603 (2019). <https://doi.org/10.11889/j.0253-3219.2019.hjs.42.020603>. (in Chinese)
 19. G.F. Zhu, R. Yan, S.H. Yu et al., An application of direct statistical method for kinetics parameters in TMSR-SF1. Nucl. Tech. **41**(05), 050603 (2018). <https://doi.org/10.11889/j.0253-3219.2018.hjs.41.050603>. (in Chinese)
 20. R.M. Ji, R. Yan, X.X. Li et al., Effect of TRISO-particles distributions in pebble fuel. Nucl. Tech. **40**(10), 100604 (2017). <https://doi.org/10.11889/j.0253-3219.2017.hjs.40.100604>. (in Chinese)
 21. K. Furukawa, K. Tsukada, Y. Nakahara, Single-fluid-type accelerator molten-salt breeder concept. J. Nucl. Sci. Technol. **18**(1), 79–81 (1981). <https://doi.org/10.3327/jnst.18.79>
 22. K. Furukawa, Y. Kato, T. Ohmichi, et al. Combined system of accelerator molten-salt breeder (AMSB) and molten-salt converter reactor (MSCR), in *Japan-US Seminar on Th Fuel Reactors, Nara* (1983), pp. 23–29
 23. K. Furukawa, Y. Kato, S.E. Chigrinov, Plutonium (TRU) transmutation and ²³³U production by single-fluid type accelerator molten-salt breeder (AMSB). AIP Conf. Proc. **346**(1), 745–751 (1995). <https://doi.org/10.1063/1.49112>
 24. C.D. Bowman, Once-through thermal-spectrum accelerator-driven light water reactor waste destruction without reprocessing. Nucl. Technol. **132**(1), 66–93 (2000). <https://doi.org/10.13182/NT00-1>
 25. Slessarev, V. Berthou, M. Salvatores, et al. Concept of the thorium fuelled accelerator driven subcritical system for both energy production and TRU incineration-‘TASSE’ (1999)
 26. H. Katsuta, T. Sasa, T. Takizuka, et al. A concept of accelerator based incineration system for transmutation of TRU and FP with liquid TRU-alloy target and molten salt blanket, in *Emerging nuclear energy systems* (1994)
 27. F. Carminati, C. Roche, J.A. Rubio, et al. An energy amplifier for cleaner and inexhaustible nuclear energy production driven by a particle beam accelerator. No. CERN-AT-93-47-ET. P00019698 (1993)
 28. M. Salvatores, I. Slessarev, A. Tchistiakov et al., The potential of accelerator-driven systems for transmutation or power production using thorium or uranium fuel cycles. Nucl. Sci. Eng. **126**(3), 333–340 (1997). <https://doi.org/10.13182/NSE97-A24485>
 29. W.S. Yang, Fast reactor physics and computational methods. Nucl. Eng. Technol. **44**(2), 177–198 (2012). <https://doi.org/10.5516/NET.01.2012.504>
 30. D. Leblanc, Molten salt reactors: a new beginning for an old idea. Nucl. Eng. Des. **240**(6), 1644–1656 (2010). <https://doi.org/10.1016/j.nucengdes.2009.12.033>
 31. V.N. Desyatnik, M.P. Vorobei, N.N. Kurbatov et al., Melting diagrams of ternary systems containing sodium and potassium chlorides, thorium tetrachloride, and plutonium trichloride. Sov. At. Energy. **38**(3), 219–221 (1975). <https://doi.org/10.1007/BF01666673>
 32. E. Indacochea, J.L. Smith, K.R. Litko et al., High-temperature oxidation and corrosion of structural materials in molten chlorides. Oxid. Met. **55**, 1–16 (2001). <https://doi.org/10.1023/A:1010333407304>
 33. D.E. Holcomb, G.F. Flanagan, B.W. Patton, et al. Fast spectrum molten salt reactor options. Oak Ridge National Lab., ORNL/TM-2011/105, 2011
 34. A. Mourgov, P.M. Bokov, Potentialities of the fast spectrum molten salt reactor concept: REBUS-3700. Energy Conv. Manag. **47**(17), 2761–2771 (2006). <https://doi.org/10.1016/j.enconman.2006.02.013>
 35. K. Yamate, S. Abeta, K. Suzuki. MOX fuel design and development consideration. No. IAEA-TECDOC-941 (1997)
 36. T. Goorley, M. James, T. Booth et al., Initial MCNP6 release overview. Nucl. Technol. **180**(3), 298–315 (2012). <https://doi.org/10.13182/NT11-135>
 37. A.G. Croff, *ORIGEN2: a revised and updated version of the Oak Ridge isotope generation and depletion code* (Oak Ridge National Lab, Oak Ridge, 1980)
 38. I. Slessarev, A. Tchistiakov. IAEA ADS-benchmark results and analysis. TCM-Meeting, Madrid, Spain, Madrid (1997)
 39. P. Seltborg. Source efficiency and high-energy neutronics in accelerator-driven systems. Dissertation, Royal Institute of Technology (2005)
 40. R. Sher. Fission-energy release for 16 fissioning nuclides. Electric Power Research Institute (1981)